Ground-state energy shift of He close to a surface and its relation with the scattering potential: A confinement model

S. A. Cruz*
Departamento de Física, Universidad Autónoma Metropolitana-Iztapalapa, Apartado Postal 55-534, 09340, México D.F., Mexico

E. Ley-Koo
Instituto de Física, Universidad Nacional Autónoma de México, Apartado Postal 20-364, 01000, México D.F., Mexico

R. Cabrera-Trujillo
Instituto de Ciencias Físicas, Universidad Nacional Autónoma de México, Apartado Postal 48-3, 62251, Cuernavaca, Morelos, Mexico
(Received 23 June 2008; revised manuscript received 4 August 2008; published 22 September 2008)

The relation between scattering potential and ground-state energy shift of a helium atom (ion) close to a surface is investigated through use of a model of spatial limitation whereby the surface is represented by an infinitely rigid planar boundary. The model of an atom confined in a semi-infinite space with a plane boundary allows the variational evaluation of the ground-state energies and wave functions for He and He^+ at different positions from the surface. The respective Born-Oppenheimer energy curves serve to model the ground-state energy shift for the elastic scattering channel in atom (ion) surface interactions. Independent calculations for the He-graphite and He-Al (111), (110), and (100) continuous planar potentials are carried out using high-quality *ab initio* calculations reported in the literature for the lowest He-C and He-Al binary interaction potentials. It is shown in this case that the He ground-state energy shift obtained within this model corresponds to an upper limit to the usual continuous planar potential. A discussion on the physical origin of this agreement is presented in terms of the static nature for the surface considered in both the hard-wall model and the atomic binary interactions used to construct the planar potentials, i.e., no account of the dynamic surface response is allowed as the projectile approaches. This is done by taking a reference pilot calculations based on electron nuclear dynamics for 100 eV He (He^+)-benzene (C_6H_6) interactions by considering the benzene molecule as a rough approximation to a local graphitic surface sector. It is found that the static planar potential provides a reasonable average representation of the interaction for neutral He, and supporting evidence for the use of the static O'Connor-Biersack potential is given. Finally, the effective scattering potential for He/He^+-Al (111) is constructed through the use of the static planar potential for He-Al (111) considering the energy shift due to the classical image interaction for He^+ approaching a perfectly Al (111) conducting plane before charge neutralization takes place. It is concluded that this scattering potential is directly related with the ground-state energy shift of the emerging already neutralized He atoms in He/He^+-Al(111) grazing scattering experiments.

DOI: 10.1103/PhysRevA.78.032905 PACS number(s): 34.35.+a, 31.15.xt

I. INTRODUCTION

Low-energy ion scattering by surfaces has been largely used as a powerful tool to study surface structure and topography, where appropriate description of the surface scattering potential is of paramount importance to simulate ion trajectories and hence relate the scattered beam profile distribution with the surface structure [1,2]. Furthermore, the development of recent accurate grazing-scattering experiments of low-energy ion beams impinging on insulator and metal surfaces has opened the possibility to survey the detailed behavior of projectile atomic states and charge exchange processes close to the surface. These kinds of experiments constitute an important source of information for understanding the basic physical phenomena taking place—at the atomistic level—in the admixture of projectile and surface electronic states. In this connection, Wethekam and Winter [3,4] have recently reported evidence on the ground-state evolution of the helium atom close to an Al(111) surface deduced from He^+ grazing-scattering experiments after Auger neutralization. This series of experiments has motivated the present study, whose aim is to survey the relation between the scattering potential and the ground-state energy shift of the He (He^+) atom (ion) induced by the spatial limitation imposed by the surface.

In this work, the surface is modeled as a hard planar boundary and the atomic ground-state energy is obtained variationally after treating the corresponding Schrödinger Hamiltonian in half-space. Clearly, in this simplified model no account of surface electronic states and possible admixture with projectile states is allowed. Interestingly, it is shown that the projectile ground-state energy shift obtained within this model is intimately related with the *static* average planar potential. To this end, highly accurate *ab initio* pairwise repulsive potentials for He-C and He-Al [5], as well as the widely used O'Connor-Biersack (OCB) universal potential [6], are used to construct the He-graphite and He-Al (111), (110), and (100) planar potentials yielding fair correspondence with the He(1*s*) ground-state energy shift calculations. It is shown that the He ground-state energy shift obtained within this model provides—in general—an upper

*cruz@xanum.uam.mx

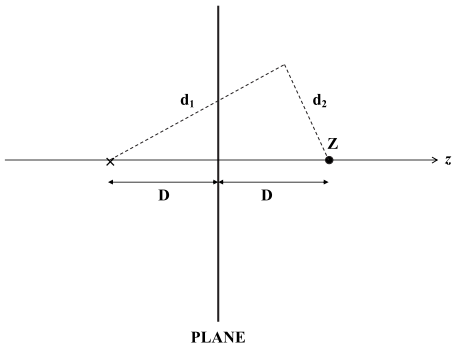

FIG. 1. Elements of the two-center coordinate system used in this work. The two centers represent the focal points of a family of ellipsoids and hyperboloids of revolution mutually orthogonal. The nuclear charge Z is located in one of the foci a distance D from the x-y plane, which is assumed to be an infinitely hard boundary. d_1 and d_2 denote the position of an electron relative to the nucleus and the other focal point.

limit to the usual continuous planar potential. A discussion on the physical origin of the observed behavior is presented in terms of the static nature of the atomic binary interactions used to construct the planar potentials as compared to their dynamic nature when the target atoms are allowed to respond as the projectile approaches. This is achieved through pilot calculations based on electron nuclear dynamics (END) [7,8] for the elastic channel in 100 eV He(He^+)-benzene (C_6H_6) interactions by considering the benzene molecule as a rough approximation to a local graphitic surface sector and comparing with the hard-plane variational calculations. Reasonable qualitative and quantitative agreement is observed between both calculations, where the relevant differences are due to the target response as the projectile approaches. It is shown—in this connection—that the OCB static planar potential provides an adequate representation of the average surface potential.

Finally, the effective scattering potential for He/He^+-Al (111) is constructed through the use of the static planar potential for He-Al (111) derived in this work, as well as with the OCB potential together with the classical image potential for He^+ approaching a perfectly Al (111) conducting plane. It is concluded that the He ground-state energy shift observed experimentally should be related with the scattering force derived from these potentials.

The paper is organized as follows. In Sec. II, the basic confinement model is presented. Section III deals with the specific discussion and results on each of the aspects mentioned in the Introduction. Finally, Sec. IV deals with the general conclusions of this work. Atomic units are used throughout unless otherwise specified.

II. THEORY

We consider the variational treatment in half-space for the He atom whose nucleus is located at a distance D from a hard-plane boundary as shown in Fig. 1. In terms of prolate spheroidal coordinates, the nuclear position corresponds to one of the foci for a family of confocal orthogonal prolate spheroids and hyperboloids defined, respectively, by the variables ξ and η as [9]

$$\xi = \frac{d_1 + d_2}{2D} \quad (1 \leqslant \xi < \infty),$$

$$\eta = \frac{d_1 - d_2}{2D} \quad (-1 \leqslant \eta \leqslant 1), \tag{1}$$

where azimuthal symmetry is considered and d_1, d_2 denote the distances of a point in space from the foci separated a distance $2D$ along the z direction. Within this coordinate representation, the plane boundary corresponds to $\eta=0$ and since we are dealing with half-space, the η-domain will be restricted to $0 \leqslant \eta \leqslant 1$.

In terms of these coordinates, the stationary Schrödinger equation for a two-electron atom of nuclear charge Z limited by a hard-plane boundary becomes

$$\left[\sum_{i=1}^{2} \hat{H}_i + \frac{1}{r_{12}}\right]\Psi = E\Psi, \tag{2}$$

where, for σ states

$$\hat{H}_i = -\frac{1}{2D^2(\xi_i^2 - \eta_i^2)}\left[\frac{\partial}{\partial \xi_i}(\xi_i^2 - 1)\frac{\partial}{\partial \xi_i} + \frac{\partial}{\partial \eta_i}(1 - \eta_i^2)\frac{\partial}{\partial \eta_i}\right] - \frac{Z}{D(\xi_i - \eta_i)} + V(\xi_i, \eta_i) \tag{3}$$

with $i=1,2$ and the confining potential given as

$$V(\xi_i, \eta_i) = \begin{cases} \infty & (\eta_i = 0; 1 \leqslant \xi_i < \infty) \\ 0 & (0 < \eta_i \leqslant 1; 1 \leqslant \xi_i < \infty), \end{cases} \tag{4}$$

where r_{12} represents the interelectronic distance in the half-space.

The solutions of Eq. (3) must satisfy the boundary conditions:

$$\Psi(\xi_1, \eta_1 = 0; \xi_2, \eta_2) = 0,$$

$$\Psi(\xi_1, \eta_1; \xi_2, \eta_2 = 0) = 0, \tag{5}$$

hence a simple—noncorrelated—trial variational wave function for the ground state of the helium atom may be cast as the product of normalized one-electron wave functions,

$$\Psi(1,2) = \Phi(\xi_1, \eta_1)\Phi(\xi_2, \eta_2) \tag{6}$$

with

$$\Phi(\xi_i, \eta_i) = N_i e^{-\alpha D(\xi_i - \eta_i)}\eta_i, \quad i = 1,2, \tag{7}$$

where the factor η_i is introduced in order to satisfy the boundary conditions of Eq. (5) and α is a variational parameter with N_i a normalizing factor.

Thus the total energy may be expressed as

$$E(\alpha, D) = T_1 + T_{12} \tag{8}$$

with T_1 and T_{12} the one- and two-electron integrals given as

$$T_1 = \langle \Psi(1,2) | \hat{h} | \Psi(1,2) \rangle,$$

TABLE I. Ground-state energy of He and He^+ as a function of distance D to a hard wall obtained in this work. Values for the corresponding variational parameter α are also provided. All values in atomic units.

D	E (He)	α (He)	E (He^+)	α (He^+)
0.01	−0.495	0.31806	−0.407	0.40877
0.05	−0.531	0.34488	−0.440	0.44773
0.1	−0.583	0.38437	−0.488	0.50609
0.5	−1.410	0.97706	−1.196	1.29681
1	−2.311	1.33942	−1.746	1.63628
2	−2.728	1.47624	−1.949	1.77712
3	−2.801	1.53331	−1.981	1.84107
4	−2.824	1.56795	−1.990	1.87808
5	−2.833	1.59064	−1.994	1.90151
10	−2.846	1.64145	−1.998	1.95017
∞	−2.857	1.67636	−1.999	1.99500

$$T_{12} = \left\langle \Psi(1,2) \left| \frac{1}{r_{12}} \right| \Psi(1,2) \right\rangle, \tag{9}$$

where

$$\hat{h} = -\frac{1}{2}(\nabla_1^2 + \nabla_2^2) - \frac{Z}{D(\xi_1 - \eta_1)} - \frac{Z}{D(\xi_2 - \eta_2)} \tag{10}$$

and using the multipolar expansion in prolate spheroidal coordinates [10],

$$\frac{1}{r_{12}} = \frac{1}{D}\sum_{l=0}^{\infty}(2l+1)\sum_{m=0}^{\infty}\varepsilon_m i^m \left[\frac{(l-m)!}{(l+m)!}\right]^2 P_l^m(\eta_1)P_l^m(\eta_2) \times Q_l^m(\xi_<)Q_l^m(\xi_>)\cos m(\varphi_1 - \varphi_2) \tag{11}$$

with $\varepsilon_0=1$ and $\varepsilon_m=2(m>0)$ and $P_l^m(z)$, $Q_l^m(z)$ the associated Legendre functions of the first and second kind, respectively. Since we are interested in the ground state, $m=0$ and the latter expression greatly simplifies. Indeed, for He^+ the above scheme simplifies considerably and its treatment is done on the same grounds.

Once a distance to the plane D is given, the total energy, as well as the variational parameter α, are obtained through the requirement

$$\left.\frac{\partial E}{\partial \alpha}\right|_D = 0. \tag{12}$$

III. RESULTS AND DISCUSSION

A. Ground-state energy evolution and dipole length

Table I displays the energy values for the ground-state evolution of He and He^+ as a function of distance to the plane together with the values of the corresponding variational parameter α. For discussion purposes and completeness, these energy values are shown graphically in Fig. 2. From this figure, a monotonic energy evolution is observed for both He (continuous line) and He^+ (dashed line) as they approach the wall and becoming very close to each other right on the wall. As expected, the ground-state energy of both systems evolves from that of an s-symmetry to a $2p\sigma$ one at the wall. It is known, however, that the ground state of hydrogenic systems sitting right on the wall corresponds to that of a p_z state [11,12] with energy $E=-Z^2/8 = -0.5$ hartree for He^+. The small energy difference observed in our calculations for this case is due to the rigidity imposed by the ansatz wave function used in Eq. (7) for very short distances to the wall. In spite of this, Eq. (7) shows to be adequate and simple enough for reliable variational calculations needed in this work within the range of distances of interest.

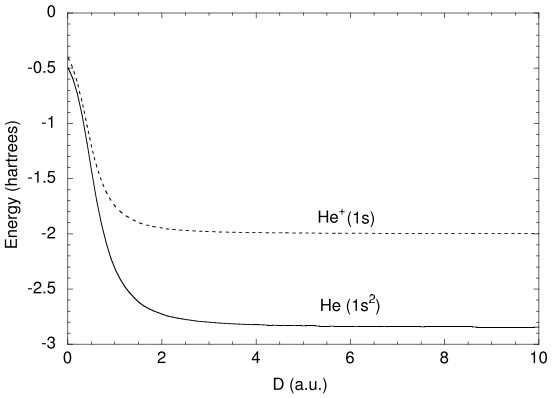

FIG. 2. He and He^+ ground-state energy as a function of distance to the wall.

Figure 3 shows contour density plots of He, as an example, for a selected set of positions relative to the wall where the evolution from s symmetry to $p\sigma$ symmetry is apparent, thus indicating a strong deformation of the electronic cloud with a consequent increase in dipole moment. A similar situation is observed for He^+.

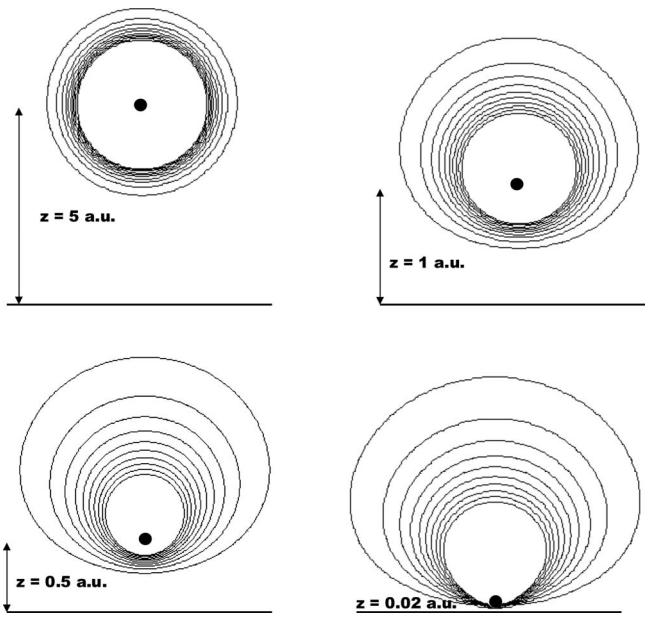

FIG. 3. Contour plots for He($1s$) showing the distortion of the electronic cloud as the atom approaches the hard wall.

TABLE II. Dipole lengths l for ground-state He and He^+ as a function of their distance D to a hard wall. Values in atomic units.

	$l=\lvert D-\langle z_e\rangle\rvert$	
D	He	He^+
0.5	0.84	0.58
1	0.41	0.30
2	0.22	0.15
3	0.14	0.10
4	0.10	0.07
5	0.08	0.06
6	0.07	0.05
7	0.06	0.04
8	0.05	0.03
10	0.04	0.02(2)

The changes in magnitude of the dipole length as a function of distance to the wall may be obtained as

$$\langle l\rangle = \langle\Psi|(D - z_e)|\Psi\rangle = D[1 - \langle\Psi|\xi\eta|\Psi\rangle] \tag{13}$$

with Ψ the optimized variational wave function for distance D for either the He or He^+ system and $z_e=D\xi\eta$ the electronic coordinate along the z axis expressed in terms of prolate spheroidal coordinates. Table II shows the magnitude of the dipole length due to distortion of the electronic cloud for He and He^+ for various distances to the plane. These quantities will be considered later in our discussion of image forces in front of a perfectly conducting plane.

B. Ground-state energy shift and planar potential

From the results shown in Table I and Fig. 2, it is clear that as the atom (ion) approaches the wall, a monotonic increase in its ground-state energy $\Delta E_s=E_s(D)-E_s(\infty)$ is observed as a result of the atom-wall interaction. Furthermore, if we consider the energy change of a system formed by a geometric planar boundary (unperturbed surface) and an approaching atom, the changes in energy of the system—hence the interaction potential—will be only due to changes in the atom energy. In spite of the obvious nature of this reasoning, it will be useful to define what we call a *static planar potential* and its relation with ΔE_s.

Consider the general case in which an atomic system A is brought close to a real surface S. Let us call $E(A,\infty)$ and $E(S,\infty)$ the energies for the isolated atom and surface, respectively. When the atom is brought to a distance D from the surface, the total energy of the compound system is $E(A^*+S^*,D)$, where A^* and S^* indicate the atom and surface final states being modified relative to their isolated condition. Then, the atom-surface interaction energy is defined as

$$V(D) = E(A^* + S^*, D) - E(A,\infty) - E(S,\infty). \tag{14}$$

At this stage, let us define a static surface as that built from either a collection of static atomic distributions or a geometric plane in such a way that no changes in its initial and final states appear due to the presence of an external perturbation. In this case, $S^*=S$, and if we consider only changes in the ground-state energy of the approaching atom, Eq. (14) reduces to

$$V(D) = \Delta E_s. \tag{15}$$

This simple expression means that for a surface with no dynamic response, the atom-surface potential is uniquely determined by changes in the atomic energy (in our case the ground-state energy shift). The consequences of this statement seem to apply to any planar potential obtained from the superposition of static pairwise interactions. To give support to this conclusion, we have constructed the continuous planar potential for He interacting with a graphitic plane and with an aluminum surface for the (111), (110), and (100) orientations as [13]

$$V(D) = 2\pi\sigma\int_0^\infty V_b(\sqrt{\rho^2 + D^2})\rho d\rho, \tag{16}$$

where σ is the surface atom density, ρ is the magnitude of the surface radial vector locating a surface element, D is the atom-surface distance, and V_b is the binary interaction potential between He and a surface atom located at a distance $r=\sqrt{\rho^2+D^2}$.

The potential V_b required in Eq. (16) has been built using the numerical values for the repulsive part of high-quality *ab initio* calculations reported by Partridge *et al.* [5] for the lowest-energy potential curves of He-C($^3\Sigma^-$) and He-Al($^2\Pi$) pairwise interactions. The aforementioned *ab initio* values are very well represented by the following analytical expression [14]:

$$V(r) = \frac{Z_1Z_2}{r}(e^{-\lambda r} + Are^{-\mu r}) \tag{17}$$

with Z_1 and Z_2 the corresponding atomic number of each species and (A,λ,μ) parameters obtained after best fit to the numerical values within the region $2.5a_0\leqslant r\leqslant 6a_0$ and to extrapolated values for the region $r<2.5a_0$ obtained through an adjusted Molière-type potential. The best-fit parameters which reproduce the *ab initio* repulsive potentials to an accuracy better than 10^{-3} a.u. are given (in atomic units) by $A=0.198\,822\,95$, $\lambda=3.029\,10$, $\mu=1.615\,50$ for He-C($^3\Sigma^-$) and $A=0.109\,596\,80$, $\lambda=2.676\,19$, $\mu=1.342\,06$ for He-Al($^2\Pi$). Using Eqs. (16) and (17) with $\sigma=0.1061a_0^{-2}$ for graphite [15] and $\sigma=(0.039\,43a_0^{-2}, 0.024\,14a_0^{-2}, 0.034\,14a_0^{-2})$ for the Al [(111), (110), and (100)] surfaces, respectively [13], the corresponding He-surface average potentials are calculated.

Figure 4 shows the behavior of the static planar interaction potential for He-graphite (long chain curve) and He-Al(111) (dotted curve), He-Al(100) (dashed curve) and He-Al(110) (short chain curve) respectively, as compared with the He($1s$) ground-state energy shift obtained with the confinement model of this work (continuous curve). Although better quantitative agreement is obtained within the confinement model and the more densely atomic packed surfaces, an important overestimate for the less packed surface is apparent. This and the quantitative discrepancies observed be-

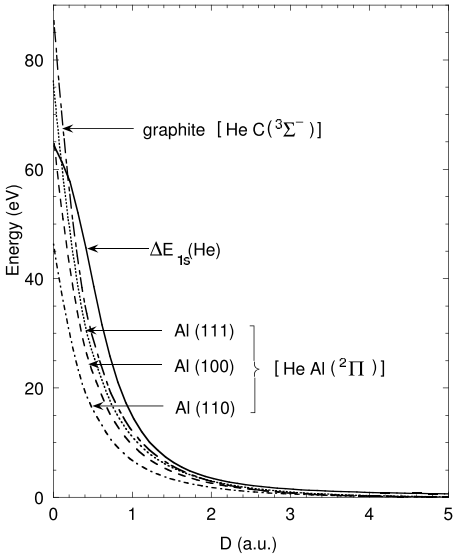

FIG. 4. Ground-state energy shift of He as a function of distance to a hard wall obtained in this work (continuous curve) compared with the continuous static planar potentials for He-graphite (long chain curve), He-Al(111) (dotted curve), He-Al(100) (dashed curve), and He-Al (110) (short chain curve).

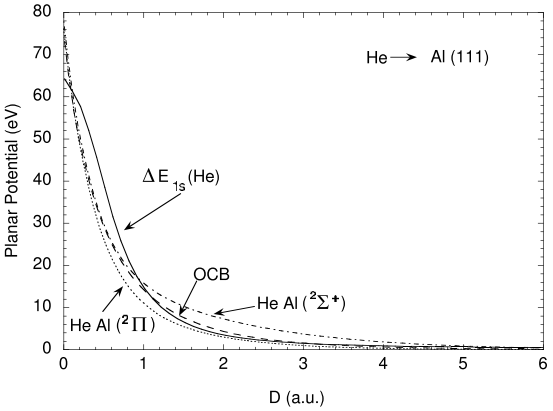

FIG. 5. Comparison of continuous static planar potentials for He-Al(111) constructed from two different molecular states for the He-Al binary interactions (chain and dotted curves). Also shown are the He ground-state energy shift obtained in this work (continuous curve) and the OCB planar potential (dashed curve).

tween both types of calculation for atom-plane distances $0 < D \leqslant 1$ may be due partly to the stringent imposition on the He ground-state energy shift due to the infinitely hard wall and to the highly repulsive core-core atomic binary interactions for very small values of D. In spite of this, the overall qualitative and quantitative correspondence between the planar potential and the ground-state energy shift curve for $D \geqslant 1$ gives supporting evidence for the validity of Eq. (15). From these results, we deem the He ground-state energy shift defines at least an upper bound to any static planar potential constructed from lowest-energy binary interactions.

The validity of Eq. (15) stems from the assumption of a static surface, i.e., with no dynamic electron response to the presence of the approaching projectile atom. At this stage, it is interesting to explore what the difference would be if the projectile-target interaction involves a different electronic state, hence mimicking a different surface state. Consider, as an example, the He-Al($^2\Sigma^+$) molecular state, which produces a higher potential energy curve than that of the He-Al($^2\Pi$) state and also reported in the *ab initio* study by Partridge *et al.* [5]. Following the same procedure as before, the static planar potential for the He-Al (111)($^2\Sigma^+$) interaction was built, where now the parameters for the corresponding repulsive binary interaction [Eq. (17)] become $A=0.075\,538\,9$, $\lambda=2.8$, and $\mu=0.919\,85$. Figure 5 shows the static He-Al($^2\Sigma^+$) (chain curve) and He-Al($^2\Pi$) (dotted curve) planar potentials obtained considering these two different states for the binary He-Al interaction. The noticeable differences between these static planar potential curves confirm the well known importance to account for the dynamic surface response to define a realistic atom-surface potential [2,16,17]. It is, however, important to take this into consideration when using static planar potentials in the description of accurate grazing-scattering experiments [3,4]. In this connection, the OCB planar potential (dashed curve)—also shown in Fig. 5—seems to provide a reasonable average representation due to its origin from the analysis of a large database of binary interaction potentials. Interestingly, the coalescence of the static planar potential curves for $0 < D < 1$ and the corresponding higher values predicted by the He ground-state shift (continuous curve) confirm the limitations of the infinitely hard-wall model in this region. Notice that the He ground-state energy shift curve for $D \geqslant 1$ lies well below the higher repulsive curve for the He-Al($^2\Sigma^+$) planar potential. This means that the He ground-state energy shift alone—as represented by Eq. (15)—and any static planar potential derived from *lowest-energy* binary interactions will provide only an approximate estimate of the atom-surface interaction potential when evolution to other surface states is allowed. That this is indeed the case may be shown as follows.

Consider the 1*s*-elastic channel evolution of the He atom interacting with the surface. Let us assume the surface is initially in state S^{I} with energy $E(S^{\mathrm{I}},\infty)$ and the He atom in its ground state with energy $E_s(\mathrm{He},\infty)$. If we allow the surface energy to evolve from state S^{I} to state S^{II} when the He atom is located at distance D from the surface, then the final energy becomes $E(\mathrm{He}+S^{\mathrm{II}},D)=E_s(\mathrm{He},D)+E(S^{\mathrm{II}},D)$, where we have invoked the static approximation for initial and final surface states. According to Eq. (14), the planar potential becomes

$$V(D) = E_s(\mathrm{He},D) + E(S^{\mathrm{II}},D) - E_s(\mathrm{He},\infty) - E(S^{\mathrm{I}},\infty)$$
$$= \Delta E_s + \Delta E(S^{\mathrm{II}},S^{\mathrm{I}}), \tag{18}$$

where the last term indicates the energy change due to the different final and initial surface states. In the He-Al(111) case, $\Delta E(S^{\mathrm{II}},S^{\mathrm{I}})>0$, thus explaining the higher values observed in Fig. 5 for the static planar potential of the He-Al($^2\Sigma^+$) states as compared to those corresponding to the He ground-state energy shift.

As a complementary test of the role of dynamical effects in the atom-surface potential and the adequacy and limitations of the model discussed here, comparison is done by performing electron nuclear dynamics [7,8] (END) calcula-

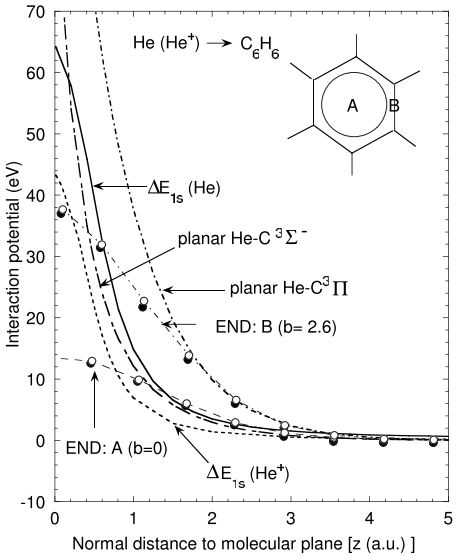

FIG. 6. Distance-dependent interaction potential for 100 eV He (open circles) and He^+ (solid circles) projectiles and a benzene molecule (C_6H_6) aimed at normal incidence to the molecular plane for impact parameters $b=0$ a.u. (label A in inset) and $b=2.6$ a.u. (label B in inset) calculated using END [7] according to Eq. (19). The distance-dependent ground-state energy shift curves for He and He^+ for a hard wall are also shown (continuous and dashed curve, respectively).

tions for 100 eV He and He^+ in their ground state colliding with a benzene molecule (C_6H_6) at normal incidence relative to the molecular plane. The planar structure of this molecule and its C-C bonding has been selected to mimic a local graphitic region so that its dynamical interaction with ground-state He (He^+) projectiles may be followed nonadiabatically and compare with the predictions of this work for the ground-state energy shift.

We first analyze the case of two extreme situations, namely, when the projectile is aimed at the center of the molecule (impact parameter $b=0$ a.u.) and at the middle of a C-C bond ($b=2.6$ a.u.). The He (He^+) projectiles and C_6H_6 molecule were initially set in their ground state with a projectile initial kinetic energy of 100 eV. For each impact parameter b, the time-dependent evolution of the $He(He^+)$-C_6H_6 supermolecule energy was recorded allowing for continuous dynamical projectile-target electronic response. The corresponding distance-dependent $He(He^+) \rightarrow C_6H_6$ interaction potential was then calculated according to Eq. (14), namely

$$V(D,b) = E[\mathrm{He}(\mathrm{He}^+) + \mathrm{C_6H_6}, D] - E[\mathrm{He}(\mathrm{He}^+), \infty] - E[\mathrm{C_6H_6}, \infty]. \quad (19)$$

Figure 6 shows the result of this calculation, where the impact points are indicated by labels A ($b=0$ a.u.) and B ($b=2.6$ a.u.) in the inset. According to this figure, the END calculation for He (open circles) and He^+ (solid circles) indicates a common behavior for the respective interaction potentials which in turn show different strengths for each impact parameter. Interestingly, the softer END potential curve ($b=0$ a.u.) shows good agreement with the He ground-state energy shift curve (continuous curve) and the He-C($^3\Sigma^-$) static planar potential (long chain curve) for $D>1.5$ a.u.. On the other hand, the more repulsive END potential curve shows better correspondence with the higher He-C $^3\Pi$ static planar potential—obtained from Eqs. (16) and (17) with $A=1.020\,802\,62$, $\lambda=3.08$, $\mu=1.754\,30$—for the same range of D values (short chain curve). This result indicates the possible involvement of other projectile-target states giving rise to the observed differences in the END interaction potentials. Finally, it is clear from this figure that the He^+ ground-state energy shift curve gives a poor description of the corresponding interaction potential since no possibility of electron capture is allowed here in the He^+-wall interaction as discussed further below.

The aforementioned different strengths in the END interaction potential for the two extreme impact parameters suggest further analysis for a collection of intermediate impact parameters in order to construct a reasonable average interaction. To this end, similar calculations were performed by aiming the $He(He^+)$ projectiles at 21 selected impact parameters relative to the symmetry molecular center at normal incidence and along a line connecting the center ($b=0$ a.u.) and the middle of a C-C bond ($b=2.6$ a.u.). Finally, the arithmetic mean interaction potential was built as

$$\langle V(D) \rangle = \frac{1}{21} \sum_{1=1}^{21} V(D, b_i) \quad (20)$$

with $V(D,b_i)$ the recorded END interaction potential for each impact parameter b_i as prescribed by Eq. (14).

Figure 7 shows the average END interaction potentials obtained from this calculation for He-C_6H_6 (open circles) and He^+-C_6H_6 (full circles). As in the previous case, a similar qualitative and quantitative trend is observed for both average interaction potentials. We note at this stage that the strongly repulsive short range core-core He-C interactions have not been included in the construction of the average END potential. Inclusion of these interactions would obviously increase considerably the average END potential for short distances ($D \leqslant 1$), thus improving the quantitative agreement with the hard-wall calculations (continuous curve) in this region. For larger distances, we deem the interaction potential is well represented by the present average END calculations. As expected in this case, the average END potential strength becomes closer to the hard-wall calculations for the He ground-state energy shift (continuous curve). The differences appearing between the average END potential and the hard-wall calculation for $1 \leqslant D \leqslant 2.5$ confirm the importance of the dynamic response of the target. Interestingly, the static He-graphite planar OCB potential (chain curve) provides an excellent agreement with the average END potential in this region and is expected to show fair agreement with the END calculations for shorter distances if the core-core interactions are included in the latter. As previously discussed in connection with Fig. 5, this result may be explained in terms of the origin of the OCB universal screening function generated as an average over a great deal of binary interactions representing different states.

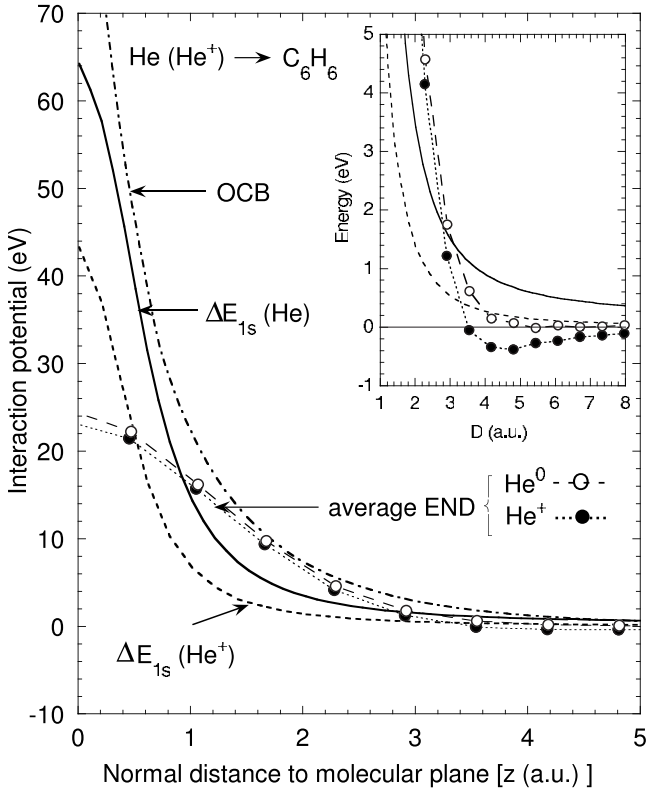

FIG. 7. Average END distance-dependent interaction potential for 100 eV He (open circles) and He^+ (solid circles) projectiles and a benzene molecule (C_6H_6) aimed at normal incidence to the molecular plane for 21 selected impact parameters. The thin dashed and dotted curves are drawn to guide the eye. Also shown are the ground-state energy shift curves for He (continuous curve) and He^+ (dashed curve) for a hard wall and the He-graphite OCB static planar potential (chain curve). The inset shows a closeup in which the admixture of projectile-target states is more strongly evidenced for the He^+ system (see text).

We may conclude at this stage that, even though we are aware of the incomplete description of a full graphitic plane by a C_6H_6 molecule, the local response of this target system provides important clues on the limitations of *single-state*-based static models for the interaction potential. Hence, a proper approach for constructing a realistic static planar potential seems to involve the generation of an average binary interaction for different states.

Following our discussion on the results presented in Fig. 7, we now focus our attention on the still poor overall description of the He^+-C_6H_6 interaction predicted by the He^+ (dashed curve) energy shift as compared with the He case. For He-C_6H_6, the interaction is repulsive as a function of D due to the neutral character of the system. However, the He^+-C_6H_6 the interaction is attractive and as the He^+ ion approaches the benzene molecule, there is a probability for electron capture which is reflected by the minimum in the interaction potential at $D \approx 4$ a.u. (see inset in Fig. 7). For smaller interaction distances, the He(He^+)-C_6H_6 system is in a combined molecular state sharing their electronic structure. At these distances, He^+ has a large probability of sharing an electron from the C_6H_6 molecule and thus resembling more the neutral He atom potential. Of course, these important dynamic effects are not contemplated by the hard-wall model for He^+, thus explaining the dramatic difference with the END calculations.

In spite of the limitations of the hard-wall model to account for projectile-target dynamical effects, the overall features of the atom-surface interaction are reasonably well represented by this simple model. Hence, we deem the hard-wall static planar potential may still provide a reasonable average description of the interaction for the already neutralized system. In particular, the He-hard-wall scattering force viewed as the slope of the interaction potential curve may be of practical interest to relate the projectile ground-state energy shift with the angular distribution of scattered atoms from a surface, as prescribed by Eq. (15). In view of the good agreement obtained for He-Al(111) among the hard-wall calculations for He, the OCB and *ab initio* planar potentials for $D \geqslant 1$, we shall consider this as a sample case for the following analysis.

C. Role of the image potential

So far we have discussed the important relationship between the static planar potential and the ground-state energy shift of helium atoms approaching the surface. We have also given some evidence on the usefulness and limitations of the hard-wall confinement model for a reasonable description of this phenomenon. Indeed, the static nature of this model prevents us from accounting for the surface response as the incoming atom (ion) approaches the surface. However, we may still explore—within the confinement model—some relevant issues concerning the role of the image potential when the hard-wall boundary is a perfect conducting one and the approaching projectile is a He^+ ion.

Let us consider a He^+ ion initially approaching the surface until the point of Auger charge neutralization by electron capture from the surface. Before neutralization, the net ion charge and distortion of its electronic cloud (dipole moment) will induce corresponding image distributions whose position—according to the jellium model—is defined in terms of an image plane located at distance z_{im}, relative to to the real surface [2,17,18]. Accordingly, the energy shift due to image interactions is measured for distances z relative to the image plane defined as $z=D-z_{\mathrm{im}}$, where D is the distance to the real surface. For simplicity, we shall consider here the point charge separation model shown in Fig. 8 for an atom (ion) whose nucleus of charge Z is located at a distance D from the surface and center of negative charge q located from the nucleus at a distance l. Within this approximation, the energy shift due to image interactions becomes

$$E_{\mathrm{im}} = -\frac{Z^2}{4z} + \frac{Zq}{2z+l} - \frac{q^2}{4(z+l)}, \tag{21}$$

where ($q=1$, $Z=2$) for He^+ and ($q=2$, $Z=2$) for He, $z=D-z_{\mathrm{im}}$ and l is given by Eq. (13). We note here that even for the neutral He system, image charge effects appear due to the distortion of the electronic cloud as a consequence of the wall confining effect (see Fig. 3). Furthermore, since we are assuming a planar boundary without structure, the He in-

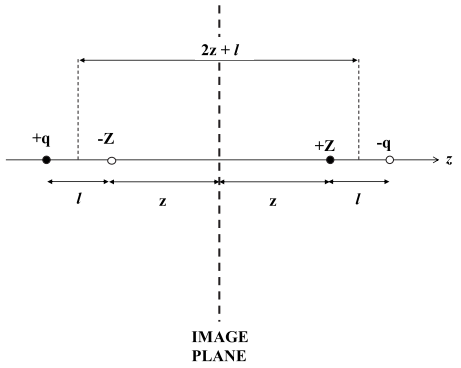

FIG. 8. Schematic representation of the point charge separation model used in this work to calculate the image interactions in Eq. (21) for an atom (ion) of nuclear charge Z located a distance z from the image plane. The dipole length l is obtained through Eq. (13) for a given distance D to the surface and such that $z=D-z_{\mathrm{im}}$, where z_{im} is the position of the image plane relative to the surface.

duced dipole moment has a different origin than the well known van der Waals interaction between a real surface and an approaching neutral atom.

We may deem the image interaction given by Eq. (21) as a first approximation to the surface response indicated by Eq. (18) considering $E(S^{\mathrm{II}},D)=E_{\mathrm{im}}$ and $E(S,\infty)=0$. Accordingly, the total planar potential [Eq. (18)] becomes

$$V(D)=\Delta E_s+E_{\mathrm{im}}, \tag{22}$$

which is valid for He^+ and He projectiles approaching a metallic surface characterized by a position z_{im} of the image plane.

Equation (22) corresponds to the widely used expression for the total surface scattering potential [17,18] once we recognize the first term in this equation as the repulsive static planar potential, as shown in the previous section.

Let us consider a He^+ ion initially approaching the surface until reaching the distance D^* where the classical image potential is assumed to saturate due to charge exchange. For $D>D^*$, the total planar potential for He^+-Al(111) is given by Eq. (22) as

$$V(\mathrm{He}^+,D)=\Delta E_s(\mathrm{He}^+)+E_{\mathrm{im}}(\mathrm{He}^+). \tag{23}$$

Once saturation takes place at $D=D^*$, the He-Al(111) potential switches on from the offset value given by $V(\mathrm{He}^+,D^*)$, i.e., the effective He-Al(111) potential [17,18] for $D\leqslant D^*$ is constructed such that

$$V_{\mathrm{eff}}(\mathrm{He},D)=V(\mathrm{He},D)-V_0, \tag{24}$$

where V_0 is the energy shift necessary to match the effective potential to that of He^+ at the saturation distance $[V_{\mathrm{eff}}(\mathrm{He},D^*)=V(\mathrm{He}^+,D^*)]$.

Strictly speaking, for $D>z_{\mathrm{im}}$ one should consider $V(\mathrm{He},D)$ in Eq. (24) as

$$V(\mathrm{He},D)=\Delta E_s(\mathrm{He},D)+E_{\mathrm{im}}(\mathrm{He},D-z_{\mathrm{im}}), \tag{25}$$

otherwise the image term becomes zero.

In order to construct the effective $\mathrm{He}/\mathrm{He}^+\mathrm{Al}(111)$ scattering potential, we have assumed $z_{\mathrm{im}}=3.3a_0$ as the position of the image plane for Al(111) [4,18] and the saturation distance $D^*\approx 5.3a_0$ $[D^*-z_{\mathrm{im}}\approx 2a_0]$ as the lowest one for the static classical image interaction limit to remain valid [17]. The dipole lengths l for He^+ and He required in Eq. (21) were extracted from the calculations leading to the results of Table II for different values of D.

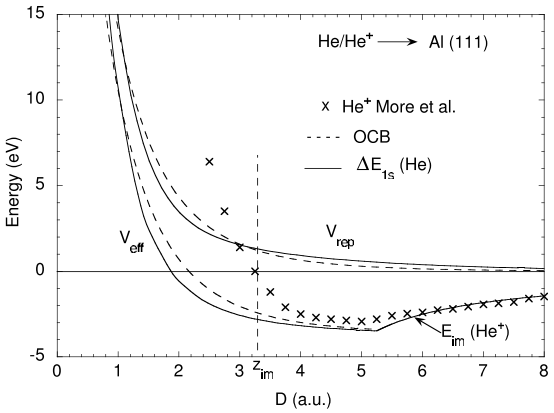

FIG. 9. Repulsive V_{rep} and effective V_{eff} scattering potentials (continuous curves) for $\mathrm{He}/\mathrm{He}^+$-Al(111) obtained from the He ground-state energy shift and considering the He^+ classical image potential before neutralization, respectively. The dashed curves represent the corresponding OCB potentials (see text). Crosses: *ab initio* calculation for He^+-Al(111) by More *et al.* [19].

For He^+, the ground-state energy shift $\Delta E_s(\mathrm{He}^+)$ in Eq. (23), as well as the corresponding dipole-induced dipole terms in the image energy contribution, were found to contribute with small corrections (less than 0.1 eV) to the charge-induced charge interaction, whereas for He, the image terms $[E_{\mathrm{im}}(\mathrm{He})$, Eq. (25)] were found to be negligible for all relevant distances $[z_{\mathrm{im}}\leqslant D\leqslant D^*]$. Accordingly, the value $V_0=3.91$ eV in Eq. (24) was used to construct the effective potential derived from the hard-wall calculations for $V(\mathrm{He},D)$ so that $V_{\mathrm{eff}}(\mathrm{He},D^*)=V(\mathrm{He}^+,D^*-z_{\mathrm{im}})=-\frac{1}{4}(D^*-z_{im})$. On the other hand, if the OCB static planar potential is used for $V(\mathrm{He},D)$, then $V_0=3.63$ eV.

For practical purposes, we have parametrized the hard-wall values for $\Delta E_s(\mathrm{He})$ within the range $0.4\leqslant D\leqslant 5.3$ through the expression

$$V(\mathrm{He},D)=Ae^{-\alpha D}+Be^{-\beta D} \tag{26}$$

with $A=99.513\,87$, $\alpha=2.156\,04$, $B=5.070\,52$, and $\beta=0.432\,39$ yielding less than 1% accuracy. Inspection of the extrapolated values obtained from this expression for $D>5.3$ indicates a reasonable quantitative description (within 0.2 eV) for $\Delta E_s(\mathrm{He})$.

Figure 9 shows the results of this work for the repulsive V_{rep} and effective total scattering potential V_{eff} (continuous curves) derived from the He ground-state energy shift [Eqs. (24) and (26)] and considering the He^+ classical image potential, respectively. The corresponding OCB repulsive and effective potentials are also shown for comparison (dashed curves) together with values extracted graphically from Ref. [4] for LCAO *ab initio* calculations of the He^+-Al(111) interaction by More *et al.* [19] (crosses). The rapid increase in

the He^+-Al(111) interaction potential predicted by the latter authors for shorter distances cannot be explained by the model proposed in this work. As expected, the OCB static planar potential provides a fair description for the repulsive and total scattering potential in agreement with the corresponding curves constructed through the He ground-state energy shift. Hence, if this potential is used to simulate the trajectories of already neutralized He ions in grazing scattering experiments, the scattering angle will be directly related with their ground-state energy shift.

IV. SUMMARY AND CONCLUSIONS

The relation between scattering potential and ground-state energy shift of a helium atom (ion) close to a surface has been investigated through use of a simple model of spatial limitation whereby the surface is represented by an infinitely rigid planar boundary. In spite of the obvious limitations of this crude model for a real surface, important features of a realistic atom-surface interaction were shown to be preserved and served as guidelines to identify the definition of a realistic static planar potential.

The He-hard-wall interaction energies as a function of wall distance were compared with independent calculations for the He-graphite and He-Al (111), (110), and (100) planar potentials. It was shown that the He atomic ground-state energy shift corresponds to an upper limit to the usual continuum planar potential constructed from the superposition of lowest-energy *ab initio* projectile-target static binary interactions (static planar potential). It has been shown that the use of higher molecular states for the projectile-target binary interaction provides different static planar potentials, which do not correspond to the He ground-state energy shift, thus mimicking the role of other helium-surface states. Further analysis of the importance of dynamic projectile-target electron response to define the interaction potential has been addressed through an electron-nuclear-dynamics (END) calculation for a local graphitic sector represented by a benzene molecule interacting with He/He^+. The local response of this target system indicated strong limitations of single-state-based static planar potentials and pointed to the need to consider an admixture of different states for projectile-target atom binary interactions in the construction of a realistic static planar potential. In this connection, the O'Connor-Biersack (OCB) potential proved to be most adequate to represent the END calculations.

In general, the poor predictions of the He^+-hard-wall interaction to account for the surface potential were discussed in terms of the importance to account for relevant projectile-surface dynamic effects such as charge neutralization, which are not included in the confinement model.

We found that in spite of the limitations of static planar potentials to account for a more realistic behavior, they can be used as an average representation of the interaction for the already neutralized system. Finally, after recognizing the good correspondence between the OCB He-Al(111) repulsive scattering potential and the He ground-state energy shift, the He/He^+-Al(111) effective potential for a perfect aluminum conducting surface was constructed considering the energy shift due to the classical image interaction for He^+. Thus, some support has been given for the use of this scattering potential in the interpretation of He/He^+-Al(111) grazing scattering experiments that are inherently related with the He ground-state energy shift.

ACKNOWLEDGMENTS

The authors wish to thank the referee for his or her very constructive criticisms, which certainly helped to improve the contents of this work. One of us (S.A.C.) deeply appreciates illuminating e-mail discussions with Professor Stephan Wethekam during the course of this work.

[1] H. Niehus, W. Heiland, and E. Taglauer, Surf. Sci. Rep. **17**, 213 (1993).
[2] H. Winter, Phys. Rep. **367**, 387 (2002).
[3] S. Wethekam and H. Winter, Surf. Sci. **596**, L319 (2005).
[4] S. Wethekam and H. Winter, Nucl. Instrum. Methods Phys. Res. B **258**, 7 (2007).
[5] H. Partridge, J. R. Stallcop, and E. Levin, J. Chem. Phys. **115**, 6471 (2001).
[6] D. J. O'Connor and J. P. Biersack, Nucl. Instrum. Methods Phys. Res. B **15**, 14 (1986).
[7] E. Deumens, A. Diz, R. Longo, and Y. Ohrn, Rev. Mod. Phys. **66**, 917 (1994).
[8] S. A. Cruz, E. Ley-Koo, and R. Cabrera-Trujillo, in *Computation in Modern Science and Engineering*, edited by T. E. Simos and G. Maroulis, AIP Conf. Proc. No. 963 (AIP, Melville, NY, 2007), p. 175.
[9] G. Arfken, *Mathematical Methods for Physicists*, 2nd ed. (Academic, New York, 1970).
[10] P. M. Morse and H. Feshbach, *Methods of Theoretical Physics, Part II* (McGraw-Hill, New York, 1953).
[11] J. D. Levine, Phys. Rev. **140**, A586 (1965).
[12] S. Satpathy, Phys. Rev. B **28**, 4585 (1983).
[13] D. S. Gemmell, Rev. Mod. Phys. **46**, 129 (1974).
[14] S. A. Cruz, L. T. Chadderton, and J. C. Barthelat, Nucl. Instrum. Methods Phys. Res. **191**, 479 (1981).
[15] R. S. Ruoff and A. P. Hickman, J. Chem. Phys. **97**, 2494 (1993).
[16] A. Schüller, G. Adamov, S. Wethekam, K. Maass, A. Mertens, and H. Winter, Phys. Rev. A **69**, 050901(R) (2004).
[17] H. Winter, J. Phys.: Condens. Matter **8**, 10149 (1996).
[18] H. Jouin, F. A. Gutierrez, and C. Harel, Phys. Rev. A **63**, 052901 (2001).
[19] W. More, J. Merino, R. Monreal, P. Pou, and F. Flores, Phys. Rev. B **58**, 7385 (1998).